Crystallization and Morphology of Semicrystalline Polyimides

Daniel P. Heberer, Stephen Z. D. Cheng,* Jeffrey S. Barley, Shawn H.-S. Lien, Robert G. Bryant, and Frank W. Harris

Institute and Department of Polymer Science, College of Polymer Science and Polymer Engineering, The University of Akron, Akron, Ohio 44325-3909

Received August 28, 1990; Revised Manuscript Received October 19, 1990

ABSTRACT: Although many semicrystalline polyimides have been synthesized, little work has been done on their solid-state characterization. This is one of the first reports concerning the crystallization behavior and crystal morphology of polyimides. In particular, this work characterizes a series of polyimides consisting of a rigid group [the imide and aromatic rings, 4,4′-oxydiphthalic anhydride (ODPA)] and a flexible linkage (an ethylene glycol sequence of n = 1, 2, or 3 repeat units). The overall crystallization behavior of the ODPA (n = 1, 2, and 3) polyimides can be described by the Avrami equation. The overall crystallization rate is dependent upon the chain flexibility and the crystallization conditions. The initial overall crystallization data (at 5% weight fraction crystallinities) show regime II/III transitions as defined by crystallization theory. The crystal morphologies of these polyimides can be observed in the micrometer range through polarized light microscopy, while resolution to a nanometer scale can be reached with transmission electron microscopy. A proposal relating the crystal morphology to the overall crystallization behavior and the crystal/amorphous interfacial structures is presented.

Introduction

For semicrystalline polymer systems, there are two important transitions: the crystallization/melting transition and the glass transition. These two transitions are attributed to different states present in the material. A transition from the liquid to the crystal state is a first-order transition (a process with an interrupted change in enthalpy, entropy, volume, etc.). Commonly, two distinct kinetic processes are discussed in isothermal crystallization experiments: the overall crystallization, which usually follows the Avrami equation,[1,2] and the linear crystal growth, which can be described by present crystallization theory.[3-8] The former includes both primary nucleation and crystal growth steps, and the latter takes into account crystal growth on an existing crystal surface. If one knows the type of primary nucleation, whether athermal nucleation (a constant number of primary nuclei) or thermal nucleation (the number of primary nuclei is a certain function of time), and the geometry of the crystal, a clear correlation between the overall crystallization and the linear crystal growth can be established.[9,10]

Recently, several reports have employed crystallization theory[3-8] to describe the overall crystallization kinetics of semicrystallization polymers. These polymers include polyethylene,[11] polypropylene,[11,12] poly(3,3-dimethylthietane),[13] cross-linked linear polyethylene,[14] and low molecular mass fractions of polyethylene.[15] The overall crystallization kinetics have been found to exhibit crystallization regimes as suggested by Hoffman and Lauritzen.[3,4]

Traditionally, a relationship between the overall crystallization kinetics and the crystal morphology may be established through the Avrami exponent n. Exact mathematical solutions are possible for one-dimensional crystallization along a line, two-dimensional crystallization, which forms a circle, and three-dimensional crystallization, which leads to spheres. Other morphologies have only been treated approximately. The equations are usually only valid at low conversion (initial crystallization) where crystallite impingement is not serious. The Avrami exponent n may show values ranging from below unity to far above six. Any one value, either integral or fractional, does not uniquely correspond to one set of conditions. Additional information about the morphology is necessary in order to more fully interpret the Avrami exponent.[16]

These crystallization and morphology studies have not, however, been extended to semicrystalline polyimides, despite the fact that the synthesis of polyimides with high glass and melting transition temperatures and good thermal stabilities has been an active area in both academic and industrial research groups. We have recently synthesized a series of polyimides consisting of a rigid group [the imide and aromatic rings, 4,4′-oxydiphthalic anhydride (ODPA)] and a flexible linkage (the ethylene glycol sequence).[17] The polymers have been designated as ODPA(n=x), where x represents the number of ethylene glycol units. The repeating unit of the polymers is

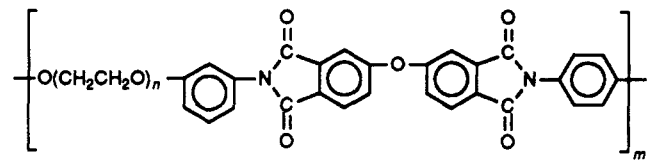

and the molecular masses are

n	MW, g/mol
1	518.5
2	562.6
3	606.6

In a recent publication,[18] we reported on the thermodynamic properties of these polyimides including the solid and liquid heat capacities, equilibrium melting temperatures, and heats of fusion. A careful study of the glass transition and melting behavior has led to a description of the interfacial region between the crystalline and amorphous states: the rigid amorphous fraction. This fraction is dependent upon the crystallization conditions (temperature and time) and also the chain flexibility.[18] The thermodynamic properties of these ODPAs are summarized in Table I. Our efforts now focus on the study of the structure formation kinetics in these polyimides,

* To whom the correspondence should be addressed.

0024-9297/91/2224-1890$02.50/0

Table I
Thermodynamic Properties of ODPA Polyimides

ODPA	T_g, K[a]	ΔC_p, J/(K mol)[a]	T_m, K[b]	ΔH_f, kJ/mol[b]
$n = 1$	450	182	613	72.5
$n = 2$	418	218	577	80.2
$n = 3$	385	254	541	88.0

[a] The data were determined for 100% amorphous polyimides. For details, see ref 18. [b] The data were determined by extrapolating to 100% crystallinity of the polyimides. For details, see ref 18.

and in this paper the crystallization kinetics and crystal morphology are discussed.

Experimental Section

Materials. The ODPAs were synthesized by following published procedures.[17] The diamines 1-(3-aminophenoxy)-2-(4-aminophenoxy)ethane (MPN1), bis[2-(3-aminophenoxy)-2-(4-aminophenoxy)ethyl] ether (MPN2), and 1-[2-(3-aminophenoxy)ethoxy]-2-[2-(4-aminophenoxy)ethoxy]ethane (MPN3) were prepared by methods developed in our laboratory.[19] 1-Methyl-2-pyrrolidone (NMP) was obtained from GAF and vacuum distilled at 353.2 K over phosphorous pentoxide.

The polyamic acids were prepared at a 15% (w/v) solid concentration by adding the diamine and NMP to a resin kettle flushed with nitrogen. An equimolar amount of dianhydride was then added to the dissolved diamine. After it was stirred for 10 h at room temperature (298.2 K), the resulting polyamic acid solution was chemically imidized with a one-to-one mixture of pyridine and acetic anhydride and then stirred overnight. The polyimides were precipitated in ethanol and collected by filtration. The polymer was dried under vacuum at 398.2 K for 24 h and then overnight under vacuum at 500 K in order to ensure complete imidization (>98%).

The polyamic acids exhibited inherent viscosities of 1.04, 1.06, and 0.68 dL/g for ODPA(n=1), -(n=2), and -(n=3), respectively, when measured in NMP at a concentration of 0.5 g/dL at 304.2 K.

Equipment and Experiments. All thermal analysis experiments were conducted on either a Du Pont 9900 thermal analyzer system or a Perkin-Elmer DSC2. Both the temperature and heat flow scales of the DSCs were calibrated at a heating rate of 10 K/min following standard procedures. Heat capacity measurements of Al_2O_3 (sapphire) on the Perkin-Elmer DSC2 were reproducible to ±0.1% based upon data from the National Bureau of Standards.[20]

The polymer samples were enclosed in aluminum pans for the DSC measurements. The weights of the reference pans and the sample pans were kept constant to a deviation of ±0.002 mg. Sample weights were in a range 10–15 mg to ensure sufficient response for measurement. Each sample was used only once to eliminate the effects of sample degradation.

Isothermal crystallization experiments were conducted by crystallizing from the melt. The samples were heated to above their equilibrium melting temperatures (see Table I) and held there for 30 s. The samples were then quickly cooled to a predetermined crystallization temperature T_c. The exothermic processes were recorded as a function crystallization time t_c. After completion of isothermal crystallization, the samples were heated to their equilibrium melting temperatures at 10 K/min without prior cooling.

Thin film samples of the ODPA were solution-cast for polarized light microscopy (PLM, Nikon Labophot-Pol) and transmission electron microscopy (TEM, JEOL-120U). The polymers were dissolved in NMP at a concentration of about 4%. Solution droplets on glass slides were put in a vacuum oven to evaporate the solvent. Only a slight increase in oven temperature was required to evaporate the solvent. The resulting films had a thickness of about 50 μm. The films were heated in a hot stage (Mettler FP-52) above their equilibrium melting temperatures (Table I) under a dry nitrogen atmosphere. They were then quickly cooled to predetermined crystallization temperatures. After a given crystallization time, the samples were quenched to dry ice temperature to fix the crystal textures. At this stage the PLM photographs were easily obtained.

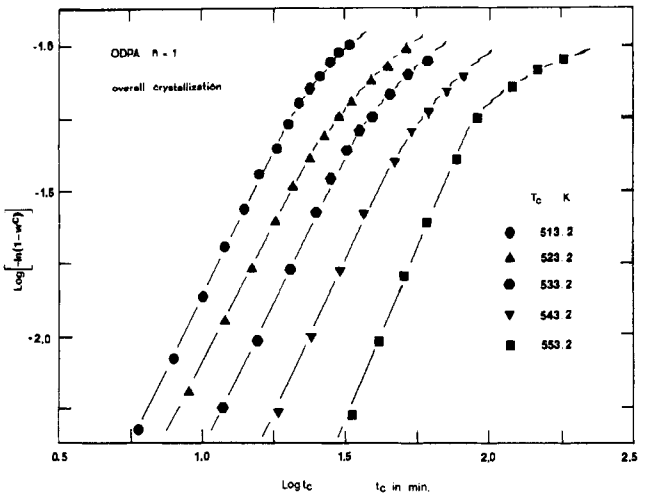

Figure 1. Avrami treatment of the overall crystallization kinetic data of ODPA(n=1) at different temperatures.

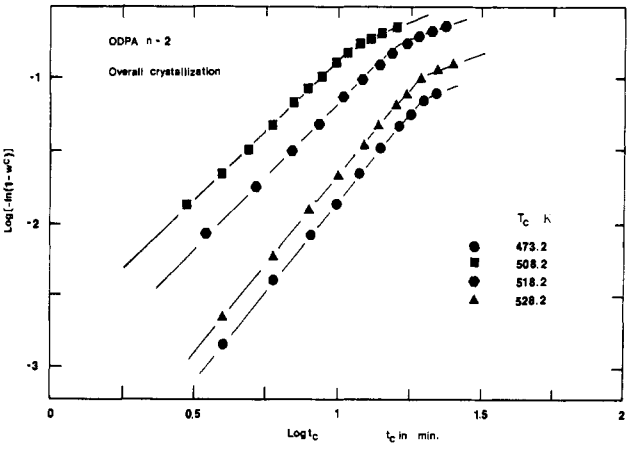

Figure 2. Avrami treatment of the overall crystallization kinetic data of ODPA(n=2) at different temperatures.

To obtain samples for TEM analysis, the sample surfaces were etched following procedures developed in our laboratory. The samples were placed in 25 mL of etchant (0.21 weight fraction C_2H_5ONa dissolved in absolute ethanol) at 298.2 K for 10 min. Temperature was controlled in a water bath to ±0.5 K under a nitrogen atmosphere. After etching, the samples were washed in absolute ethanol and then dried. The chemical reaction responsible for the etching is perceived to involve an attack of the organic base on C—H leading to $CH{=}CH_2$ chain scission.[21] The samples were then replicated by using acetylcellulose film (Bioden R.F.A.). The films were placed in a vacuum evaporator for oblique shadowing (30 °C) with a heavy-metal alloy (Pd/Au, 0.4/0.6) followed by perpendicular coating with carbon. The acetylcellulose films were removed from the surface replica by dissolving in acetone. The replicas were deposited on copper grids for investigation in the TEM operated at an accelerating voltage of 100 kV.

Results

Overall Crystallizations. The Avrami treatment can be used to describe our crystallization data. Figure 1 shows a plot of log [-ln (1 - w^c)] versus log t_c for ODPA(n=1) at different crystallization temperatures. Two crystallization processes can be observed. A primary crystallization process occurs first, with an Avrami exponent n = 1.8–2.3. This process develops about 80% of the total crystallinity. The increase in crystallinity then levels off, indicating a second process with an Avrami exponent n smaller than 1. A similar situation can be found in the overall crystallization of ODPA(n=2), as shown in Figure 2. For ODPA(n=3), the overall crystallization behavior is rather

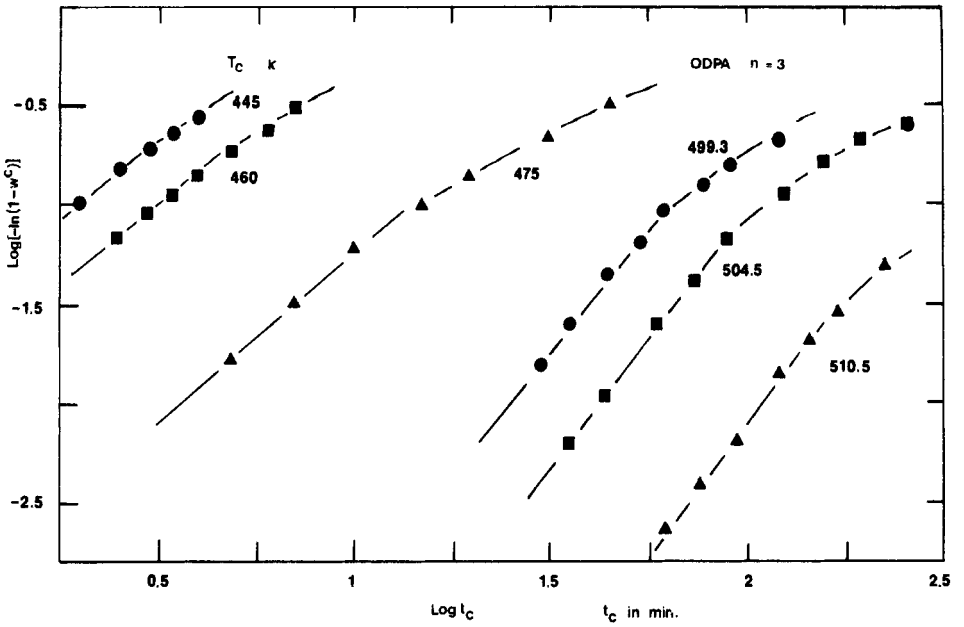

Figure 3. Avrami treatment of the overall crystallization kinetic data of ODPA(n=3) at different temperatures.

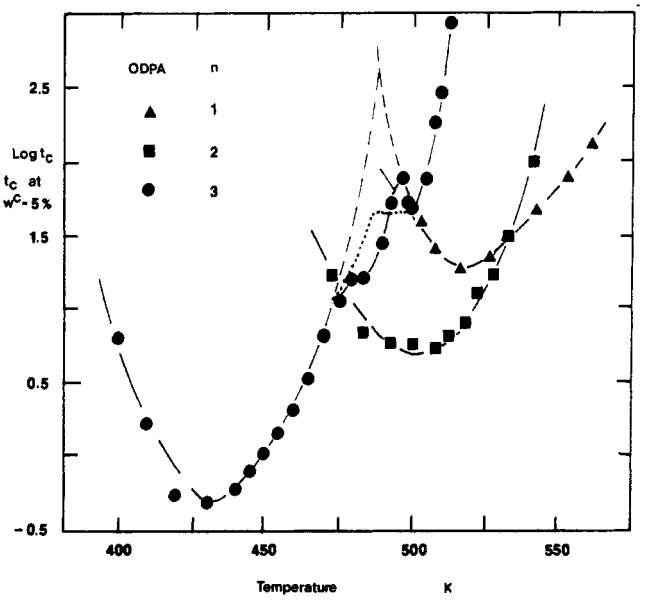

Figure 4. Relationships of the logarithm of the time required to reach a weight fraction crystallinity of 5% versus crystallization temperature for ODPA(n=1), -(n=2), and -(n=3).

complicated since two crystalline forms exist. The Avrami exponent of the primary crystallization ranges between 0.7 and 2.1. The secondary crystallization process can be observed at high crystallization temperatures (Figure 3). Of special interest is that the transitions between primary and secondary crystallization processes in these ODPA polyimides occur at the times when the low melting peaks start appearing, as described in ref 18.

Figure 4 demonstrates the relationship between the logarithm of the time required to reach 5% weight fraction crystallinity and crystallization temperature for ODPA-(n=1), -(n=2), and -(n=3). It is clear that ODPA(n=1) and -(n=2) show normal crystallization behavior. There is a minimum of log t_c for each polymer, corresponding to the fastest crystallization rate. For ODPA(n=1), the fastest crystallization rate can be observed at T_c = 513 K, and for ODPA(n=2) it is at T_c = 500 K. Figure 4 shows interesting behavior for ODPA(n=3). Two minima can be found at T_c = 429 and 500 K. The minimum at the lower temperature corresponds to the fastest crystallization rate of the low-temperature crystalline form, and the minimum at the higher temperature corresponds to the fastest crystallization rate of the high-temperature crystalline form. Of special interest is the temperature region between T_c = 468 and 500 K. If one extends the experimental crystallization data (log t_c) for these two individual processes symmetrically as shown in Figure 4 (dashed lines), one can calculate the growth contributions of both crystalline forms from these curves. Under the assumption that these two forms grow independently, one can obtain the dotted lines shown in Figure 4. Nevertheless, the experimental data do not fit the dotted line. This indicates that in this temperature region the growth of these two crystalline forms is not independent. At the low-temperature side, the crystallization rates for both forms are faster than when they grow independently. At the high-temperature side, these rates are slower than when they grow independently. The absolute values of the logarithmic crystallization time are of special importance because they closely relate to chain flexibility. The more flexible chains (more ethylene glycol units) have faster overall crystallization rates. Finally, changes in the Avrami exponent n are parallel to the change in log t_c as shown in Figure 4. A faster crystallization rate generally corresponds to a lower Avrami exponent.

Crystal Morphologies. Figure 5 shows the crystal morphologies for ODPA(n=1) crystallized at three different temperatures. At the lowest crystallization temperature, T_c = 493.2 K (Figure 5a), there is a compacted spherulitic texture with a regular Maltese extinction cross. After impingement the spherulitic size is generally about 5 μm. With an increase in the crystallization temperature to 513.2 K (Figure 5b), the Maltese extinction cross is still observable, and additional banding patterns within the spherulites gradually appear. At the highest crystallization temperature of 543.2 K (Figures 5c and its enlargement Figure 5d), it is evident that, besides the Maltese extinction cross, the spherulitic texture changes to a more open one. The radiation type of lamellar aggregation is clear, but with distinctive banding patterns. The banding spacing (distance between neighboring banding patterns) in the spherulites is constant and found to be about 0.4 μm (Figure 5d).

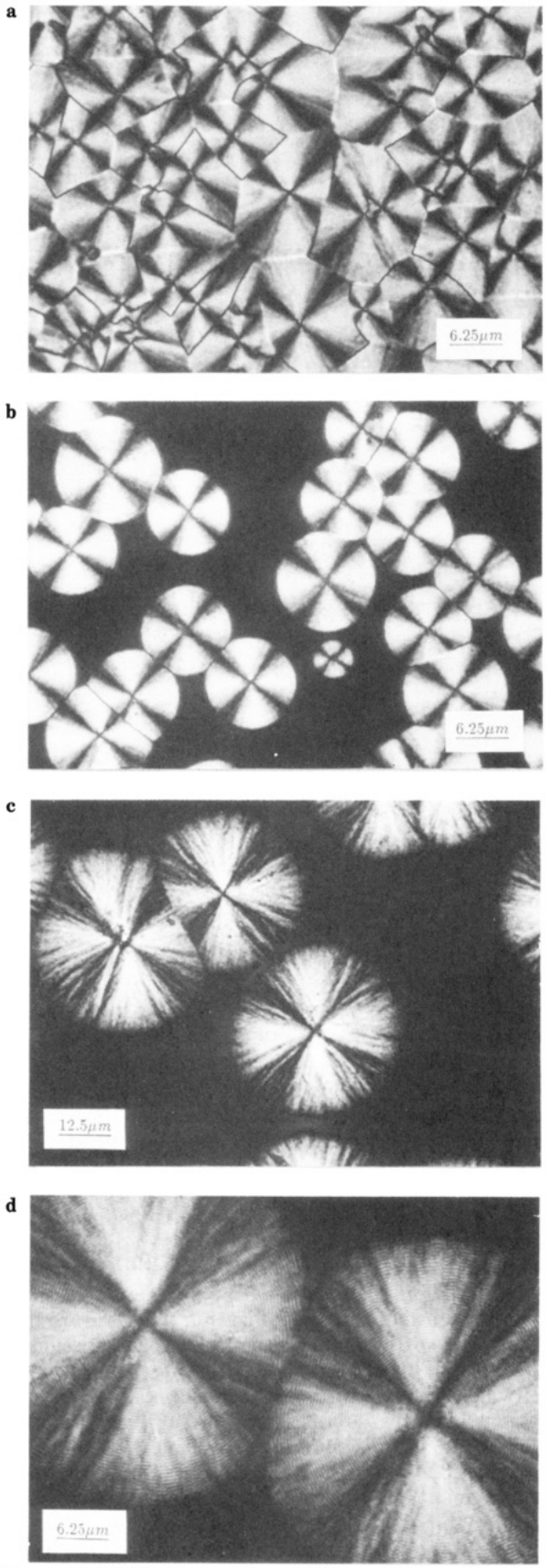

Figure 5. PLM observations of the crystal morphologies of ODPA(n=1) crystallized at (a) 493.2 K, (b) 513.2 K, and (c, d) 543.2 K.

Parallel studies on TEM for these polyimides have also been conducted. Parts a and b of Figure 6 represent the crystal morphologies of the ODPA(n=1) crystallized at a low temperature (493.2 K) and a high temperature (543.2 K), respectively. Because of the finer resolution of TEM compared to that of PLM, detailed lamellar crystal textures can be observed. From Figure 6a, it is evident that rather compact spherulitic textures form at this low crystallization temperature with a heavy degree of lamellar branching. The long spacing is around 24.5 nm. It corresponds to a lamellar thickness of about 4.4 nm with 18% crystallinity.

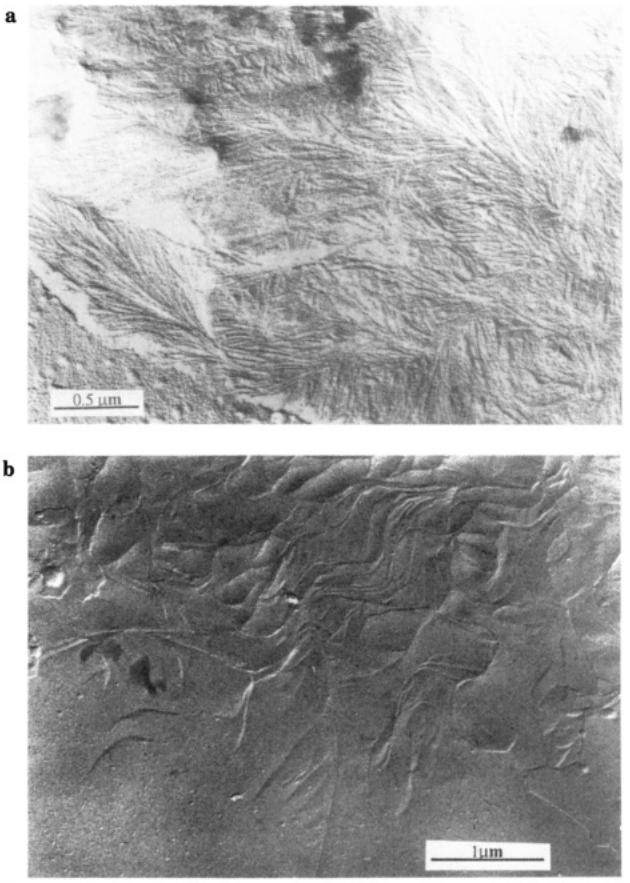

Figure 6. Crystal textures of ODPA(n=1) crystallized at (a) 493.2 K and (b) 543.2 K observed by TEM.

Increasing the crystallization temperature to 543.2 K changes the crystal morphology to that shown in Figure 6b. This Figure represents an edge of one spherulitic texture, for which two distinct features can be compared relative to Figure 6a. First, its lamellar thickness is now about 11 nm and exhibits a lower branching density. Second, at the crystal growth front, a relatively open texture can be observed. Leading single lamellar crystal growths can be observed as shown in Figure 6b. The later growth is comprised of lamellae filled in between the leading lamellae.

Parts a, b, and c, d of Figure 7 show under PLM the crystal morphology changes of ODPA(n=2) crystallized at 493.2, 523.2, and 543.2 K, respectively. Changes similar to those in ODPA(n=1) can be observed. The radiation growth of lamellar aggregation in ODPA(n=2) seems prominent. At the highest crystallization temperature, both radiation growth and banding patterns can be seen. The banding spacing in this case, however, is about 0.6 μm (Figure 7 d), which is about 1.5 times larger than that for n = 1.

For ODPA(n=2), the change of crystal morphology with crystallization temperature under TEM is very similar to the case of ODPA(n=1), as illustrated by Figure 8, parts a (T_c = 493.2 K) and b (T_c = 543.2 K). An increase in lamellar thickness of the crystal with temperature is evident. The crystal texture also undergoes the change

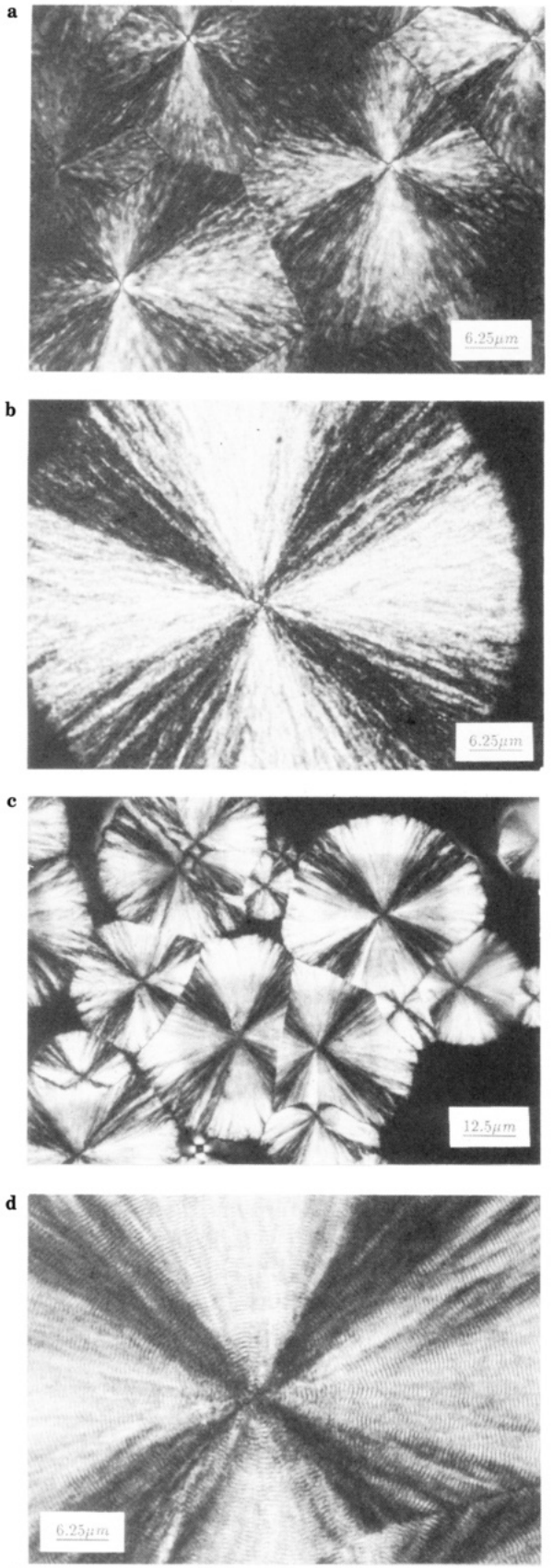

Figure 7. PLM observations of the crytal morphologies of ODPA(n=2) crystallized at (a) 493.2 K, (b) 523.2 K, and (c, d) 543.2 K.

from a compact (Figure 8a) to a relatively open one (Figure 8b) in the spherulites.

ODPA(n=3) shows different crystal morphologies as shown in Figure 9. This polymer has two crystalline forms

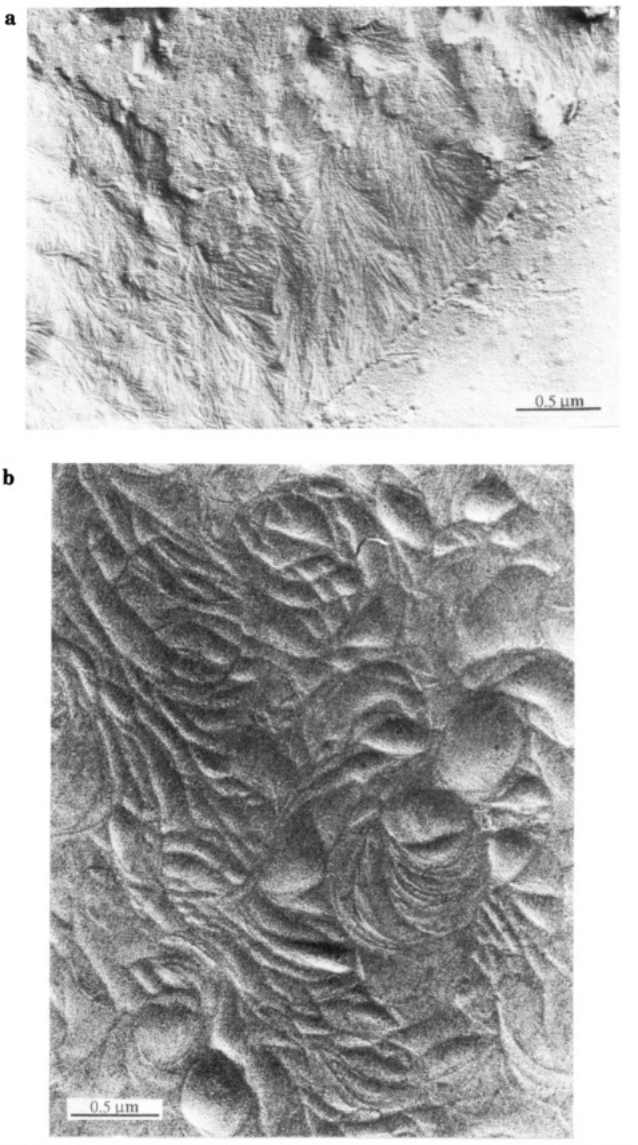

Figure 8. Crystal textures of ODPA(n=2) crystallized at (a) 493.2 K and (b) 543.2 K observed by TEM.

and there is a morphology difference between these forms. Figure 9a represents the crystal morphology at a low crystallization temperature (468.2 K) where the low-temperature crystal form grows. One can clearly see that only axialites are formed. Most of the axialites show elliptic shapes, though some are cyclic. This indicates two-dimensional axialites since these two different shapes are caused by viewing the axialites from different directions. With an increase in the crystallization temperature by 5 K to 473.2 K, two different crystal morphologies are evident (Figure 9b). This crystallization temperature is in the region where the two different forms coexist (see Figure 4). One is axialitic (as was seen in Figure 9a); the other displays a radiation type of growth without regular Maltese extinction patterns. A mixture of these two morphologies in one crystalline domain can also be seen, indicating an interference between these two types of growth. Subsequent heating determined that the axialites melt at around 500 K and the radiation type of crystals melt at 530 K. At T_c = 488.2 K, where only the high-temperature crystalline form grows, one finds that indeed only one type of morphology remains. The axialites cannot be observed (Figure 9c). If the crystallization temperature is increased to 513.2 K, a more open texture is found. The radiation type of lamellar aggregations is treelike (Figure 9d). In a relatively thicker film, one can even see

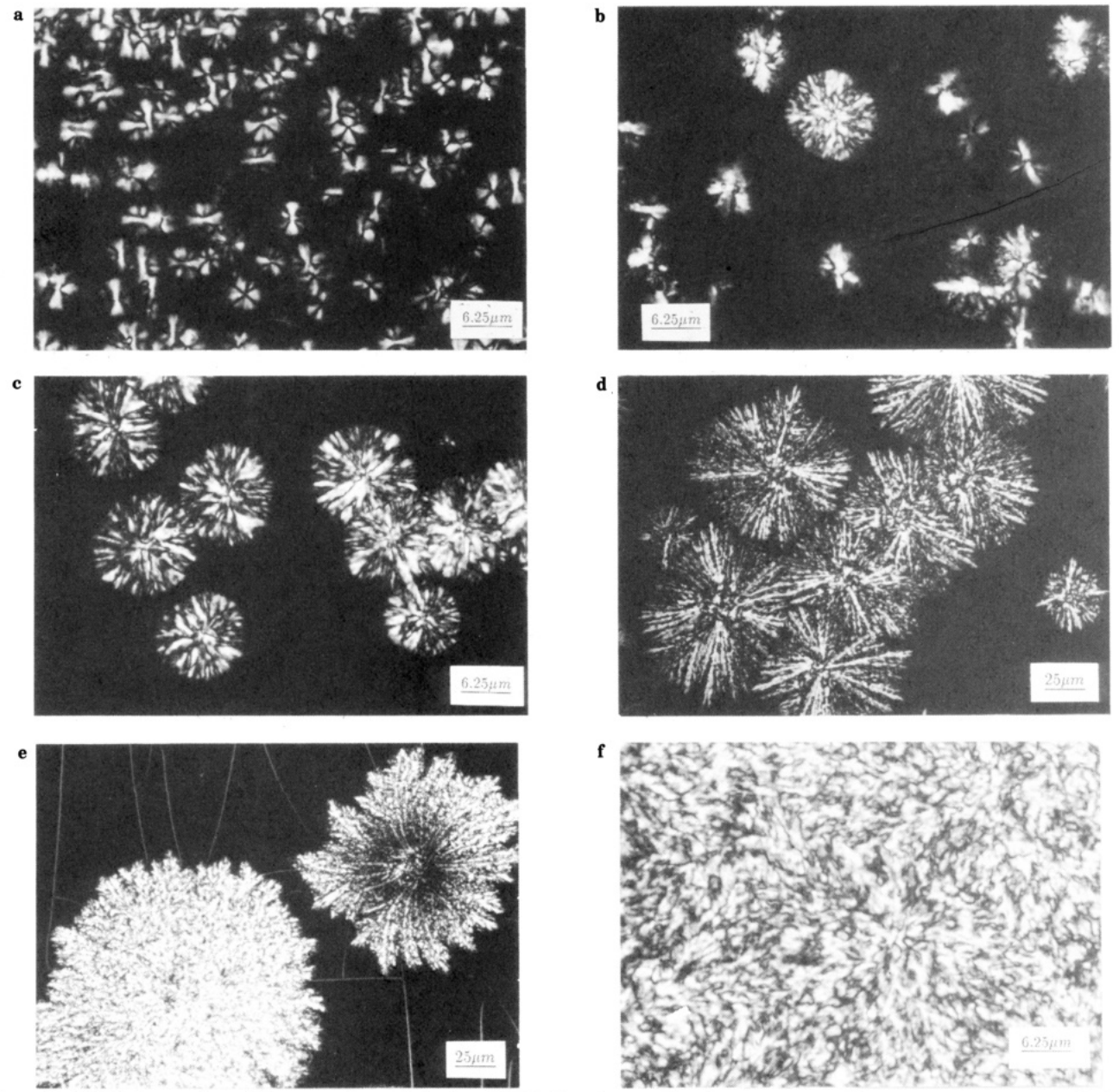

Figure 9. PLM observations of the crystal morphologies of ODPA(n=3) crystallized at (a) 468.2 K, (b) 473.2 K, (c) 488.2 K, and (d–f) 513.2 K.

flowerlike growth (upper right of Figure 9e). Figure 9f is an enlarged center portion of the lower left texture in Figure 9e. No radiation type of lamellar aggregations can be observed, but instead there is a random stacking of many crystal layers. Additionally, no banding pattern appears in the ODPA(n=3) at high crystallization temperatures.

Figure 10a,b shows the crystal morphology of ODPA(n=3) crystallized at a low temperature of 468.2 K under TEM. One can classify the overall morphology to be axialitic. In fact, Figure 10a presents a view that is edge on to an axialite, and Figure 10b shows a somewhat more mature one. "Eye structures" are apparent near the center of the axialites where the primary nucleation was initiated. This is the usual case for axialitic growth. The crystal texture is quite compact, with an average length for lamellar branching of 0.75 μm. An average distance between two neighboring lamellar crystals at the growth front is 0.13 μm. This distance decreases rapidly toward the crystal center. The long spacing is about 23 nm, which is equivalent to a lamellar thickness of 6.0 nm based on the crystallinity information.[18]

Crystallization at 513.2 K yields the textures of lamellar crystals as shown in Figure 10c,d. This represents the high-temperature form. Figure 10c gives a relatively large viewing area (small magnification) involving a tip of the treelike crystal texture shown in Figure 9d. With increasing magnification (Figure 10d), one can see that the crystal growth front is rather open. Individual lamellar crystals grow with less branching. The average length of lamellar branching now increases to 1.4 μm. The average distance between two neighboring lamellar crystals at the growth front is 0.36 μm and decreases slowly toward the crystal center. The combination of less branching and more separated lamellae leads to a more open texture. The long spacing is about 37 nm, leading to a lamellar thickness of 13 nm.[18]

Regime Analysis. Several reports have indicated that the overall crystallization data can show regime transition behavior.[11-15] We also try the regime analysis on our overall crystallization data based on crystallization theory.[3-8] It is known that one can plot the relationship between log $G - \log \Delta T + U^*/[2.303R(T_c - T_\infty)]$ and $1/[T_c(\Delta T)f]$, where

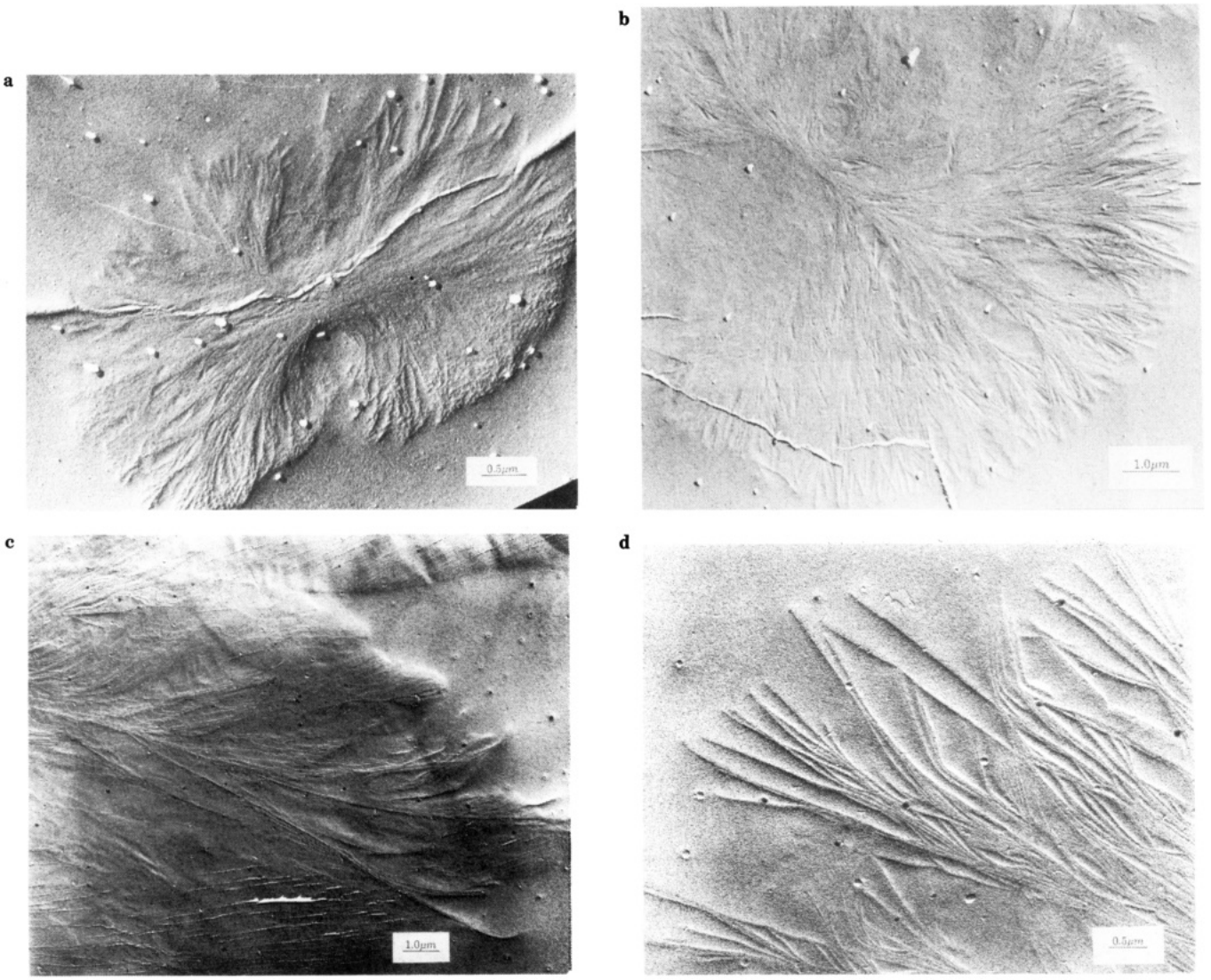

Figure 10. Crystal textures of ODPA(n=3) crystallized at (a, b) 468.2 K and (c, d) 513.2 K observed by TEM.

G is the linear crystal growth rate, U^* represents the activation energy, $T_\infty = T_g - 30$ K, and $f = 2T_c/(T_m^\circ + T_c)$. The subtraction of log ΔT from log G was recently derived by Hoffman and Miller.[8] In order to treat the overall crystallization data, the linear crystal growth rate, G, must be replaced by the term $[t_c(0.05)]^{-1}$, where $t_c(0.05)$ is the time required to reach a 5% weight fraction crystallinity. The activation energy we used is the universal value of 6.28 kJ/mol proposed by Hoffman et al.[22] The equilibrium melting temperatures of these polyimides are listed in Table I. In the case of ODPA(n=3), a complication is introduced by the existence of two different crystalline forms. Below about T_c = 470 K, the crystals that grow are mainly the low-temperature form, and we did not have its equilibrium melting temperature and heat of fusion. The equilibrium melting temperature of the low-temperature form was assumed to be 500 K, about 10 K above the observed melting temperature.[18] This value of 10 K is the difference between the equilibrium melting temperature of the high-temperature form and the observed melting temperature from our experiments. Since the low-temperature form is a relatively disordered state, the heat of fusion is assumed to be the same as for the high-temperature form. When the overall crystallization data at high temperatures (above T_c = 500 K) is treated in a similar manner, the equilibrium melting temperature of the high-temperature form is used (Table I). In this temperature region, only the high-temperature crystal form grows. Figure 11 shows the relationship between log $[t_c(0.05)]^{-1}$ – log $\Delta T + U^*/[2.303R(T_c - T_\infty)]$ and $1/[T_c(\Delta T)f]$ for these ODPA(n=3); only the overall crystallization data of T_c < 470 K and T_c > 500 K are

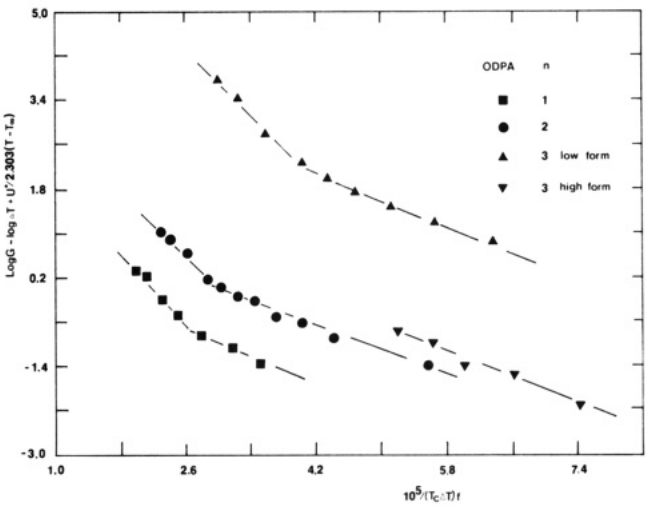

Figure 11. Relationship between log $[t_c(0.05)^{-1} - \log \Delta T + U^*/[2.303R(T_c - T_\infty)]$ and $1/[T_c(\Delta T)f]$ for the overall crystallization kinetics of ODPA(n=1), -(n=2), and -(n=3) polyimides crystallized from the melt. The plots are based on the crystallization theory proposed by Hoffman et al.[3-8]

Table II
Overall Crystallization Kinetic Data of ODPA Polyimides

ODPA(n=x)	regime	10^{-5}Kg, K^2	$\sigma\sigma_e$, erg^2/cm^4	ratio (III/II)
n = 1	II	1.771	750	2.02
	III	3.577	760	
n = 2	II	1.563	740	2.01
	III	3.146	740	
n = 3 (low form)	II	1.532	730	2.03
	III	3.104	740	
n = 3 (high form)	II	1.363	650	

included. The overall crystallization data in between 470 and 500 K are complicated due to the mixed growth of the low-temperature and high-temperature crystal forms. Therefore, this treatment is difficult to apply in this temperature region. If one uses different values of the activation energy U^* (we have tried from 4 to 10 kJ/mol) while fixing other parameters, the ratios of the two slopes are no longer equal to two.

For ODPA(n=1), a regime transition is found at ΔT = 75 K (T_c = 538 K). On the basis of the features of this transition, one can assign it as being a regime II/III transition. Similar regime II/III transitions for ODPA-(n=2) and -(n=3) can also be observed. They occur at ΔT = 70 K (T_c = 507 K) and ΔT = 65 K (T_c = 476 K) for these two polymers, respectively. However, for the high-temperature crystal form of ODPA(n=3), only regime II is found; no transition in this temperature region can be seen. The slopes Kg of each crystallization regime shown in Figure 11 are listed in Table II. For all three polymers, the ratios between the slopes of regimes II and III are essentially close to two as expected by crystallization theory.[3-8] Furthermore, from these slopes the product of the lateral and fold surface free energies $\sigma\sigma_e$ can be calculated from the equation

$$Kg = ib_o\sigma\sigma_e T_m^\circ/(\Delta h_f)k \quad (1)$$

where i = 2 for regime II growth and i = 4 for regime III growth. From our wide-angle X-ray diffraction (WAXD) measurements, the lengths of b_o are 0.514, 0.517, 0.543, and 0.541 nm, for ODPA(n=1), -(n=2), and low- and high-temperature forms of (n=3), respectively, if one assumes that crystal growth is along the (010) crystalline plane.[23] Furthermore, one can convert the heats of fusion (ΔH_f) in Table I from kJ/mol to the units of erg/cm^3 by knowing the crystallographic densities of these ODPAs from the WAXD data (ρ_c = 1.381, 1.433, 1.386, and 1.388 g/cm^3 for these ODPA, respectively[23]). The products of the surface free energies $\sigma\sigma_e$ are listed in Table II. This product decreases slightly with an increasing number of ethylene glycol units. This indicates that the product of the surface free energies, and in particular the fold surface free energy, is chain flexibility dependent if one considers that lateral surface free energy remains constant. For ODPA(n=3), crystallization at high temperatures leads to a growth of the high-temperature form, and the product of the surface free energies is relatively lower (about 12–13%) than for its low-temperature form.

Discussion

The crystal morphology of these ODPA polyimides when crystallized from the melt, whether spherulitic, axilitic, or even more open treelike textures, depends upon the chain flexibility and crystallization conditions. For ODPA(n=1) and -(n=2), the regular Maltese extinction crosses observed under PLM are clearly due to an isotropic radiation type of crystal growth. At high temperatures, additional banding patterns indicate a twisting of crystallographic orientation about radii that apparently reflects cooperative twisting of the radiating lamellar crystals about their axes of fastest growth. Its occurrence implies a high degree of cooperation in packing the lamellae into fairly compact textures. The packing of lamellae has clearly been documented by our TEM observations as shown in Figures 6b and 8b. It is also interesting that the banding spacing increases slightly with crystallization temperature in both cases. This behavior is commonly observed in banded spherulites.[24,25] On the other hand, the spacing in ODPA-(n=2) is larger than that in ODPA(n=1). Both facts indicate that the twisting of the lamellar crystals is not only temperature but also chain flexibility dependent. In the case of ODPA(n=3) the axialitic texture essentially obscures the Maltese extinction crosses, as usually reported.[26] The open, treelike texture at high crystallization temperatures eliminates the cooperative twisting of the radiating lamellar crystals, and therefore there is no banding pattern.

From our TEM observations it is particularly interesting to find that the distance between two neighboring lamellar crystals at the growth front is larger than that within the crystal textures. Apparently, the development of these crystal textures begins by the formation of radially elongated leading lamellar crystals, which is followed by subsequent growth between the leading lamellae. At low crystallization temperatures where compact textures are seen, the subsequent growth is due mainly to a branching mechanism, which develops concomitantly within these leading lamellae and usually occurs not far behind them. At high crystallization temperatures, more open textures appear. The subsequent growth is dominantly the "in-filling" type. This type grows considerably later.[27] These observations and analyses may further help our understanding of the formation of spherulitic and axialitic morphologies.[28] The effort to establish a relationship between the Avrami exponent and the crystal morphology has been a long time endeavor in the study of polymer crystallization.[16] However, this relationship is commonly restricted by two factors. First, the Avrami equation is only a simple data-fitting treatment if one does not have a microscopic kinetic model in mind. Second, one has to know the exact nucleation type and crystal morphology. In our ODPA polyimides, the nucleation type can be determined through PLM observations. Spherulitic, axialitic, and more open treelike textures represent well-defined geometries of crystal growth. As a result, these textures correspond well to the growth dimension illustrated by the Avrami exponents.[16] The secondary crystallization process exhibited by these polyimides occurs after spherulite impingement and is very similar to that behavior commonly observed in polymer crystallization. The starting time of the secondary crystallization process corresponds well to the appearance of the low-melting peak in our crystal melting study.[18] This indicates, again, that the low-melting peak materials are formed later in the overall crystallization process and are closely related to the branching and/or in-filling type of lamellar growth.

The effect of chain flexibility on the rate of overall crystallization is apparent, as shown in Figure 4. For a given supercooling, the time required to reach 5% weight fraction crystallinity decreases with increasing number of ethylene glycol units. The overall crystallization rate is predominantly controlled by the primary nucleation and crystal growth steps. Both of these steps should be functions of the chain flexibility. More rigid polymer chains exhibit a higher viscosity and therefore slower molecular motion. From our PLM observations, ODPA(n=3)

has the highest primary nucleation density and ODPA(n=1) the lowest, at the same supercooling. On the other hand, to crystallize a rigid-chain molecule requires overcoming a higher nucleation barrier during crystal growth. This is due to the deposition of a longer stem on the crystal surface as a single step of the growth. We believe that the combination of these two factors leads to the slower overall crystallization rate for the more rigid ODPA(n=1) polyimide.

Incidently, the observation of the mixtures of two morphologies in one ODPA(n=3) crystalline site (see Figure 9b) at the low-temperature side of the region between 468 and 500 K can be understood as annealing of the low-temperature form to the high-temperature form crystal during isothermal crystallization. If the high-temperature crystal form is present in the initial growth, subsequent growth of this crystal form is probable. This leads to a faster crystallization when compared with the assumed independent growths of these two crystal forms, as shown in Figure 4. On the other hand, at the high-temperature side in this region, growth of the low-temperature crystal form is quickly annealed to the high-temperature crystal form. As a consequence, the resultant overall crystallization is slower than that of the assumed independent growths of the two crystal forms.

Finally, in many semicrystalline polymers the existence of an interfacial region, the rigid amorphous fraction, has been documented. This region lies between the crystal and the isotropic amorphous states.[29-32] In these ODPA polyimides we have also observed this interfacial region.[18] It is evident that this fraction is dependent upon the chain flexibility and the crystallization conditions. Increasing the chain flexibility and crystallization at high temperatures decreases the amount of this fraction. Since the rigid amorphous region must be on a nanometer scale, it should be closely related to the lamellar crystals that subsequently grow within the crystal textures. At low crystallization temperatures, these subsequent lamellae are formed mainly through branching with relatively small crystal sizes and, correspondingly, a relatively large interfacial area. Fast crystallization with irregular chain conformations leads to a decrease in the amount of adjacent reentry folding in the crystals and an increased interfacial region percentage, such as tie molecules etc. Random stacking of the lamellae may also cause internal stresses, which generally concentrate at the interfacial region. At high crystallization temperatures, in-filling lamellae grow more or less independently. Relatively large portions of adjacent reentry folding in the crystals are expected. This internal stress must thus decrease. Therefore, the rigid amorphous fraction should depend upon the crystal size and the degree of irregularity of the lamellar crystal stacking. The quantitative evaluation of the rigid amorphous fraction and the morphology changes in these polymers may be the first step in assessing the study of the interfacial region.

Acknowledgment. This research is supported by Edison Polymer Innovation Center (EPIC) through its research grant of polyimide studies and the Exxon Educational Foundation.

References and Notes

(1) Avrami, M. *J. Chem. Phys.* **1939**, *7*, 1103.
(2) Avrami, M. *J. Chem. Phys.* **1940**, *8*, 212.
(3) Lauritzen, J. I., Jr.; Hoffman, J. D. *J. Appl. Phys.* **1973**, *44*, 4340.
(4) Hoffman, J. D.; Frolen, L. J.; Ross, G. S.; Lauritzen, J. I., Jr. *J. Res. Natl. Bur. Stand.* **1975**, *79A*, 671.
(5) Frank, F. C. *J. Cyst. Growth* **1974**, *18*, 111.
(6) Hoffman, J. D. *Polymer* **1982**, *23*, 656.
(7) Hoffman, J. D. *Polymer* **1983**, *24*, 3.
(8) Hoffman, J. D.; Miller, R. L. *Macromolecules* **1988**, *21*, 3038.
(9) Cheng, S. Z. D.; Wunderlich, B. *J. Polym. Sci., Polym. Phys. Ed.* **1986**, *24*, 595.
(10) Lopez, L. C.; Wilkes, G. L. *Polymer* **1988**, *29*, 106.
(11) Allen, R. C.; Mandlekern, L. *Polym. Bull.* **1987**, *17*, 473.
(12) Janimak, J. J.; Cheng, S. Z. D. *Polym. Bull.* **1989**, *22*, 95.
(13) Lazcano, S.; Fatou, J. G.; Marco, C.; Bello, A. *Polymer* **1988**, *29*, 2076.
(14) Phillips, P. J.; Lambert, W. S. *Macromolecules* **1990**, *23*, 2075.
(15) Fatou, J. G., Marco, C.; Mandelkern, L. *Polymer* **1990**, *31*, 890.
(16) Cheng, S. Z. D. *J. Appl. Polym. Sci. Sympo.* **1989**, *43*, 315.
(17) Harris, F. W.; Lien, S. H.-S. *PMSE Proc., Am. Chem. Soc.* **1989**, *60*, 197.
(18) Cheng, S. Z. D.; Heberer, D. P.; Lien, S. H.-S.; Harris, F. W. *J. Polym. Sci., Polym. Phys. Ed.* **1990**, *28*, 655.
(19) Harris, F. W.; Sridhar, K. *Polym. Prepr., Am. Chem. Soc. Polym. Chem. Div.* **1988**, *29* (2), 304.
(20) Ginnings, D. C.; Furukawa, G. T. *J. Am. Chem. Soc.* **1953**, *75*, 522.
(21) Cheng, S. Z. D.; Bu, H.-S.; Wunderlich, B. *J. Polym. Sci., Polym. Phys. Ed.* **1988**, *26*, 1947.
(22) Hoffman, J. D.; Davis, G. T.; Lauritzen, J. I., Jr. In *Treatise on Solid State Chemistry*; Hannay, N. B., Ed.; Plenum: New York, 1976; Vol. 3, Chapter 7.
(23) Heberer, D. P. Ph.D. Dissertation, Department of Polymer Science, The University of Akron, Akron, OH 44325-3909; 1990.
(24) Phillips, P. J.; Rensch, G. J.; Taylor, K. D. *J. Polym. Sci., Polym. Phys. Ed.* **1987**, *25*, 1725.
(25) Keith, H. D.; Padden, F. J., Jr.; Russell, T. P. *Macromolecules* **1989**, *22*, 666.
(26) Cheng, S. Z. D.; Bu, H. S.; Wunderlich, B. *J. Polym. Sci., Polym. Phys. Ed.* **1988**, *26*, 1947.
(27) Keith, H. D.; Padden, F. J., Jr. *Polymer* **1986**, *27*, 1463.
(28) Cheng, S. Z. D.; Barley, J. S.; Giusti, P. A. *Polymer* **1990**, *31*, 845.
(29) Cheng, S. Z. D.; Cao, M. Y.; Wunderlich, B. *Macromolecules* **1986**, *19*, 1868.
(30) Cheng, S. Z. D.; Wunderlich, B. *Macromolecules* **1987**, *20*, 1620.
(31) Cheng, S. Z. D.; Wu, Z. Q.; Wunderlich, B. *Macromolecules* **1987**, *20*, 2082.
(32) Cheng, S. Z. D.; Wunderlich, B. *Macromolecules* **1988**, *21*, 879.